2014

Upwelling rebound, ephemeral secondary pycnoclines, and the creation of a near-bottom wave guide over the Monterey Bay continental shelf

Cheriton, Olivia M.; McPhee-Shaw, Erika E.; Storlazzi, Curt D.; Rosenberger, Kurt J.; Shaw, William J.; Raanan, Ben Y.

AGU Publications

Cheriton, O. M., E. E. McPhee-Shaw, C. D. Storlazzi, K. J. Rosenberger, W. J. Shaw, and B. Y. Raanan (2014), Upwelling rebound, ephemeral secondary pycnoclines, and the creation of a near-bottom wave guide over the Monterey Bay continental shelf, Geophys. Res. Lett., 41, 85038511.

http://hdl.handle.net/10945/57133

AGU PUBLICATIONS

Geophysical Research Letters

RESEARCH LETTER
10.1002/2014GL061897

Key Points:
- Under upwelling, a near-bed pycnocline appeared on outer Monterey Bay shelf
- High-frequency nonlinear internal waves of elevation propagated near seabed
- Regional upwelling dynamics control propagation of internal waves over the shelf

Correspondence to:
O. M. Cheriton,
ocheriton@usgs.gov

Citation:
Cheriton, O. M., E. E. McPhee-Shaw, C. D. Storlazzi, K. J. Rosenberger, W. J. Shaw, and B. Y. Raanan (2014), Upwelling rebound, ephemeral secondary pycnoclines, and the creation of a near-bottom wave guide over the Monterey Bay continental shelf, *Geophys. Res. Lett.*, *41*, 8503–8511, doi:10.1002/2014GL061897.

Received 16 SEP 2014
Accepted 20 NOV 2014
Accepted article online 25 NOV 2014
Published online 5 DEC 2014

The copyright line for this article was changed on 7 JAN 2016 after original online publication.

Upwelling rebound, ephemeral secondary pycnoclines, and the creation of a near-bottom wave guide over the Monterey Bay continental shelf

Olivia M. Cheriton[1], Erika E. McPhee-Shaw[2], Curt D. Storlazzi[1], Kurt J. Rosenberger[1], William J. Shaw[3], and Ben Y. Raanan[4]

[1]Pacific Coastal and Marine Science Center, U.S. Geological Survey, Santa Cruz, California, USA, [2]Shannon Point Marine Center, Western Washington University, Anacortes, Washington, USA, [3]Oceanography Department, U.S. Naval Postgraduate School, Monterey, California, USA, [4]Moss Landing Marine Laboratories, California State University, Moss Landing, California, USA

Abstract Several sequential upwelling events were observed in fall 2012, using measurements from the outer half of the continental shelf in Monterey Bay, during which the infiltration of dense water onto the shelf created a secondary, near-bottom pycnocline. This deep pycnocline existed in concert with the near-surface pycnocline and enabled the propagation of near-bottom, cold, semidiurnal internal tidal bores, as well as energetic, high-frequency, nonlinear internal waves of elevation (IWOE). The IWOE occurred within 20 m of the bottom, had amplitudes of 8–24 m, periods of 6–45 min, and depth-integrated energy fluxes up to 200 W m^{-1}. Iribarren numbers (<0.03) indicate that these IWOE were nonbreaking in this region of the shelf. These observations further demonstrate how regional upwelling dynamics and the resulting bulk, cross-margin hydrography is a first-order control on the ability of internal waves, at tidal and higher frequencies, to propagate through continental shelf waters.

1. Introduction

Internal waves are widespread and important physical features of the coastal ocean [*Lamb*, 2014]. When internal waves break or become highly nonlinear, they can drive changes in vertical water column structure and effectively transport both heat and organisms [*Pineda*, 1999]. Most observations of high-frequency, nonlinear internal waves are those of steep depressions propagating along a shallow pycnocline just below the surface-mixed layer. Rarer are observations of internal waves of elevation (IWOE), which occur when a pycnocline is in close proximity to the seafloor. Nonlinear IWOE can be highly turbulent and, as they propagate over a continental shelf, are thought to increase suspended particulates in the bottom boundary layer (BBL) and contribute to transporting and mixing dense ocean water with shelf waters [*Bogucki et al.,* 1997; *Klymak and Moum,* 2003; *Scotti and Pineda,* 2004; *Moum et al.,* 2007]. Internal waves of depression convert to IWOE as they propagate from deep to shallow water, as has been observed in a wide variety of environments, such as the shallow regions of Massachusetts Bay [*Scotti and Pineda,* 2004], the St. Lawrence Estuary [*Bourgault et al.,* 2007], and in the South China Sea [*Orr and Mignerey*, 2003; *Fu et al.,* 2012]. Over the shelf of Monterey Bay, California, *Carter et al.* [2005] observed downslope propagating IWOE that transformed into waves of depression upon reaching deep canyon waters. During winter months when energetic mixing and/or downwelling result in a deepened pycnocline, IWOE have been observed over continental shelves off both Oregon [*Klymak and Moum*, 2003; *Moum et al.,* 2007] and California [*Bogucki et al.,* 1997].

Here we present observations taken from the southern Monterey Bay shelf in the late fall of 2012 that show the propagation of IWOE along a secondary, near-bottom pycnocline that appeared during several sequential upwelling periods. These results demonstrate how the upwelling-driven variation in stratification over the shelf is a key component to the formation of wave guides that allow the propagation of internal wave energy at both tidal and higher frequencies.

2. The Field Experiment

Moorings were deployed on the southern Monterey Bay shelf from 3 to 28 October 2012, at two different sites: S70 and S90 on approximately the 70 and 90 m isobath, respectively (Figure 1). These

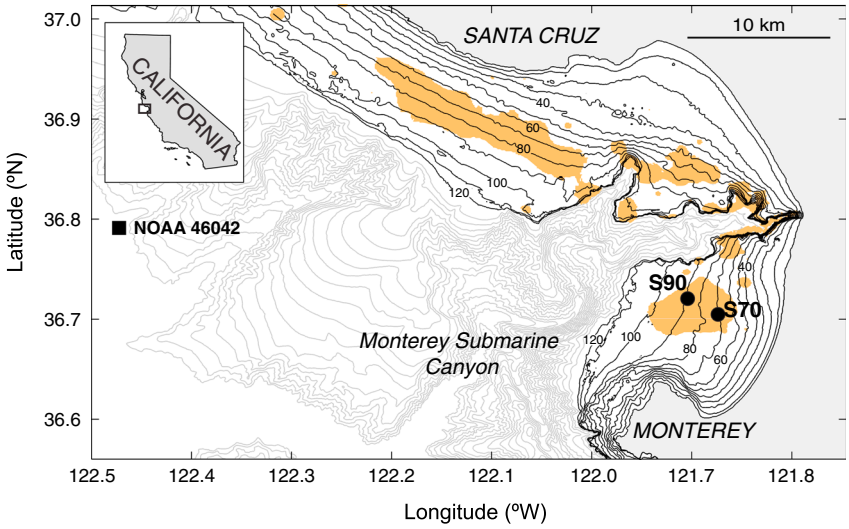

Figure 1. Map of Monterey Bay, California showing location of S90 and S70 mooring sites on the southern shelf, as well as the offshore NOAA 46042 buoy (square). The approximate location of the midshelf mud belt is indicated by the orange overlay (data originally published in *Edwards* [2002]). Black bathymetric contours are in 10 m increments from 0 to 120 m, and gray contours are in 100 m increments from 200 to 2000 m. The inset map shows location of Monterey Bay along the coast of California, USA.

two sites were located in the midshelf mud belt, which is primarily comprised of fine grain (mud and silt) sediment. Each site had a thermistor chain and a tripod with an upward looking Teledyne RD Instruments 300 kHz WorkHorse Sentinel acoustic Doppler current profiler (ADCP). At S70, the ADCP collected current profiles with 2 m vertical bins every minute, with 25 pings per ensemble. The S70 thermistor chain had 14 SeaBird SBE 39 thermistors sampling every 30 s; they were spaced 5 m apart from 1.5 to 61.5 m above bottom (mab); the thermistors at 1.5, 31.5, and 61.5 mab also measured pressure. An autonomous Brooke Ocean SeaHorse vertical profiler outfitted with a SeaBird SBE 19plus conductivity-temperature-depth (CTD) logger was also deployed at S70 and collected hourly profiles of the water column between 9 mab and 1.5 m below the surface. The CTD on the profiler collected measurements at 4 Hz, for a vertical resolution of approximately 0.15 m. For full details on the operation of the autonomous profiler, see *Cheriton et al.* [2014]. The three instrument platforms at S70 (thermistor chain, tripod, and profiler) were located ~400 m from each other. At S90, the ADCP measured current velocity profiles with 2 m vertical bins in 2 min ensembles, with 60 pings per ensemble. Also on the tripod, an RBR thermistor measured temperature every 30 s, and at 3 mab a SeaBird SBE37 CT sensor measured temperature and salinity every 3 min. The S90 thermistor chain had eight RBR thermistors sampling every 30 s; they were placed every 10 m between 10 and 70 mab. The S90 mooring platforms were first deployed on 11 April 2012, resulting in a nearly 6 month long record. Here we only focus on the one month period of overlap between the S90 and S70 records.

Water column stratification at S70 and S90 was evaluated using the squared Brunt-Väisälä frequency, $N^2 = -g/\rho_o(\Delta\rho/\Delta z)$, where g is the gravitational acceleration, ρ_o is the mean water density over a vertical profile, and ρ is the density at a given depth, z. For S70, density profiles from the high vertical resolution profiler were used to compute N^2, while for the S90 site we estimated density based on the thermistor chain measurements, using a constant salinity of 33.5. While the S90 N^2 values should only be taken as conservative approximation of N^2, there is good agreement between the S90 and S70 N^2 records (pycnoclines are of same order of magnitude), despite the lack of vertical resolution in the S90 N^2 calculations. For example, the time-averaged maximum N^2 value measured in the lower half of the water column from 6 to 11 October is $3.9 \times 10^{-4}\,s^{-2}$ at S70 and $2.0 \times 10^{-4}\,s^{-2}$ at S90. The N^2 values were then used with current shear, $S = \sqrt{(dU/dz)^2 + (dV/dz)^2}$, to calculate the Richardson number, $Ri = N^2/S^2$, a measure of the ratio of buoyancy forces associated with density stratification and shear instabilities.

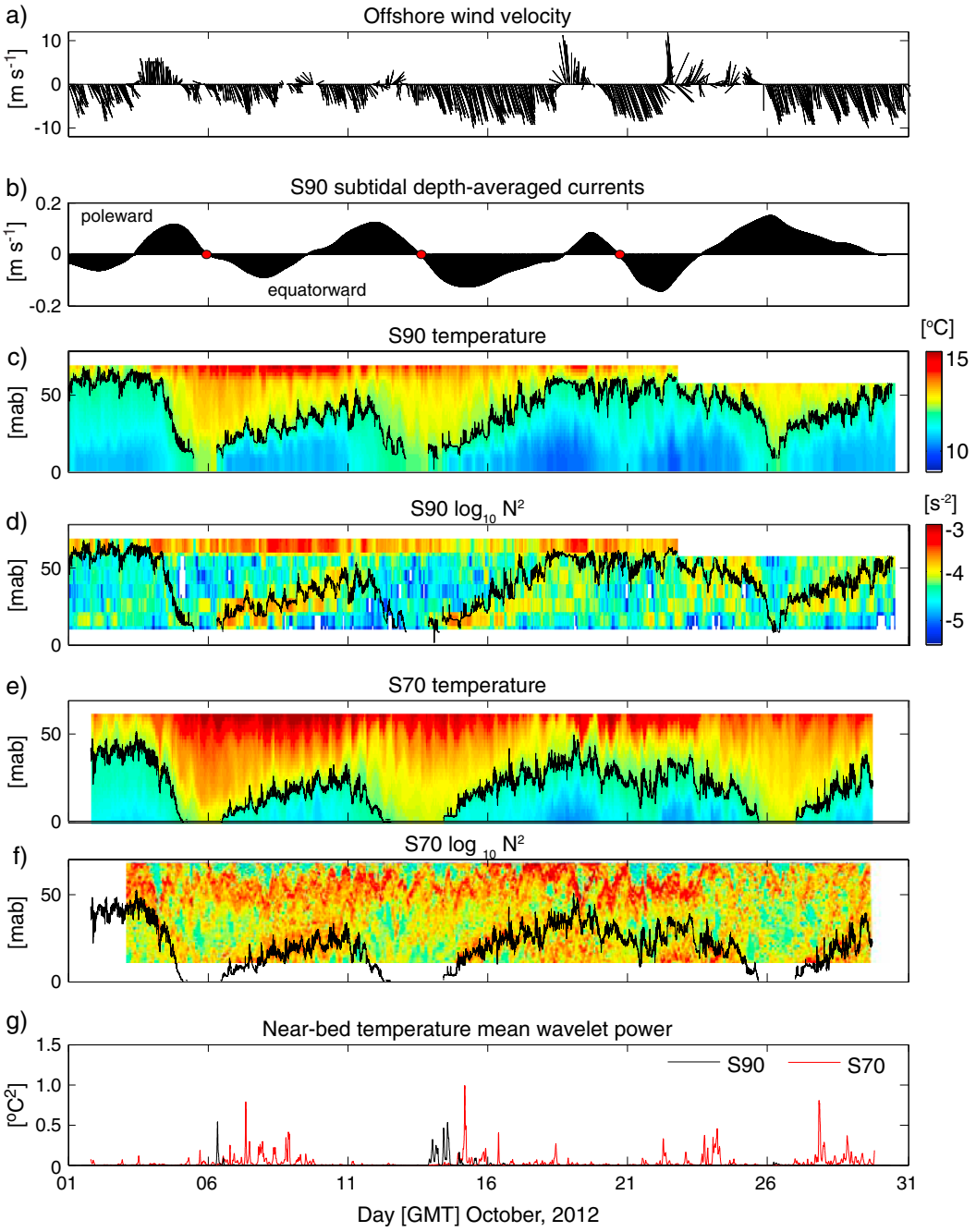

Figure 2. Complete study period record from 1 to 31 October 2012, showing: (a) offshore wind velocity, with the stick vector direction indicating wind heading (upward = northward/poleward); (b) the depth-averaged subtidal currents measured at S90 with red dots indicating the start of an upwelling period; (c) water column temperature at S90; (d) the squared Brunt-Väisälä frequency, N^2, in $\log_{10}$ scale at S90; (e) water column temperature at S70; (f) N^2 in $\log_{10}$ scale at S70; the 12°C isotherm is overlaid in Figure 2a–2f (black line) and indicates the approximate depth of the near-bed, secondary pycnocline. (g) The frequency-averaged wavelet power associated with high-frequency (10–30 min) fluctuations in bottom temperature at S90 (black) and S70 (red).

In general, portions of the water column where $Ri < 0.25$ are considered unstable and prone to shear instabilities [*Mann and Lazier*, 2006].

The localized, temporal variations in temperature variance associated with different frequencies were investigated using the Morlet nonorthogonal, continuous wavelet transform [*Torrence and Compo*, 1998].

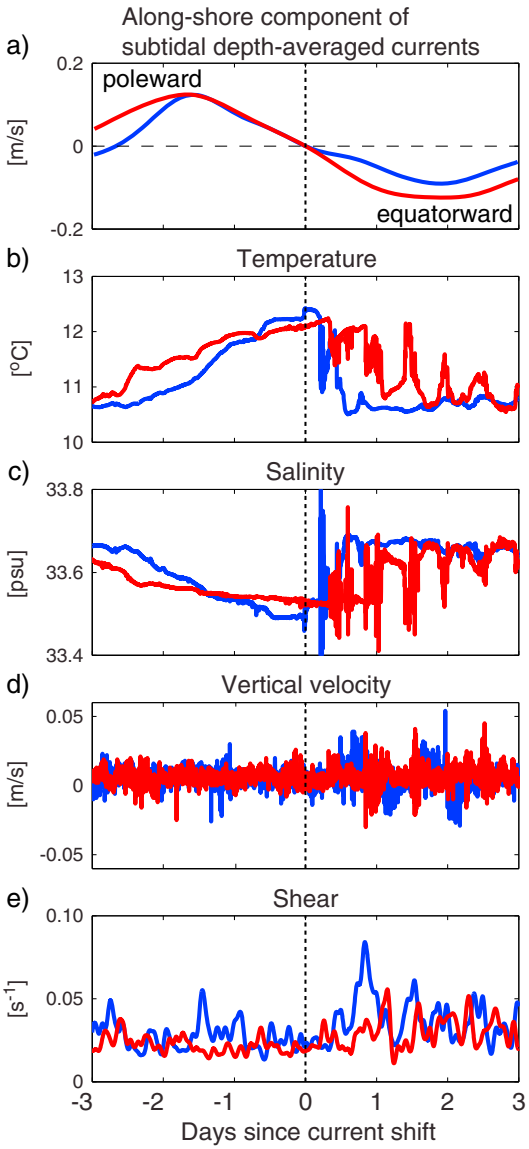

Figure 3. Near-bed properties measured at S90 during the first two upwelling rebound periods, where day 0 is the time when the depth-averaged subtidal currents switched from poleward to equatorward. Time series are shown from 3 days before and 3 days after the current shift: (a) along-shore component of depth-averaged subtidal currents, (b) temperature and (c) salinity from 3 mab, (d) vertical velocity and (e) low-pass-filtered shear from 10 mab.

Using this method, we calculated the mean wavelet power (units of variance) for specifically targeted frequencies associated with short-period internal wave oscillations ($\omega \leq N$), and the M_2 semidiurnal internal tide (period ~12.5 h). This method was applied to temperature, current velocity components, as well as isotherm time series. All three time series types yielded similar results; for simplicity, only the temperature time series wavelets are presented herein.

Wind and wave data were obtained from the NOAA National Data Buoy Center buoy #46042 (www.ndbc.noaa.gov), located approximately 50 km west-northwest from Monterey, California (Figure 1).

3. Observations

A series of oscillations between upwelling and downwelling/relaxation states occurred throughout the 1 month study period. In general, upwelling periods in Monterey Bay are marked by persistent equatorward (northwesterly) winds offshore, with corresponding equatorward subtidal flow over the shelf (Figures 2a and b). We defined the start of each upwelling period as the onset of equatorward subtidal flow; the month-long study period captured three distinct upwelling periods, with start times of 6, 13, and 20 October (red dots on Figure 2b). At the start of these upwelling periods, cold water infiltrated the bottom portion of the water column over the shelf (Figures 2c and 2e). Between these upwelling periods, the flow within the bay shifted poleward and within 1–2 days the water column rapidly warmed. These observations are in agreement with previous descriptions of the water column response to upwelling dynamics over the Monterey Bay shelf [*Rosenfeld et al.,* 1994; *Storlazzi et al.,* 2003]. During this 1 month study, under upwelling, the infiltration of cold water onto the shelf brought with it a secondary pycnocline, which first appeared at S90, then at S70, gradually shoaling as the cold water reached farther up into the water column (Figures 2d and 2f; approximate depth of the secondary pycnocline depth is indicated by the 12°C isotherm). This secondary, near-bottom pycnocline coexisted with, and was of similar strength ($N^2 \sim 4 \times 10^{-4}\,s^{-2}$) to the near-surface pycnocline, and it appeared on the shelf through multiple, sequential upwelling periods. The water below the secondary pycnocline was dense and unstratified.

The progression from a nonupwelling to upwelling state was a rapid, highly dynamic event in the lower water column (Figure 3). These "upwelling rebounds" began less than 12 h after the shift from poleward to equatorward subtidal currents and were characterized by a rapid drop (rise) in bottom temperature (salinity), followed by elevated near-bed shear and vertical velocities. In the case of the second upwelling

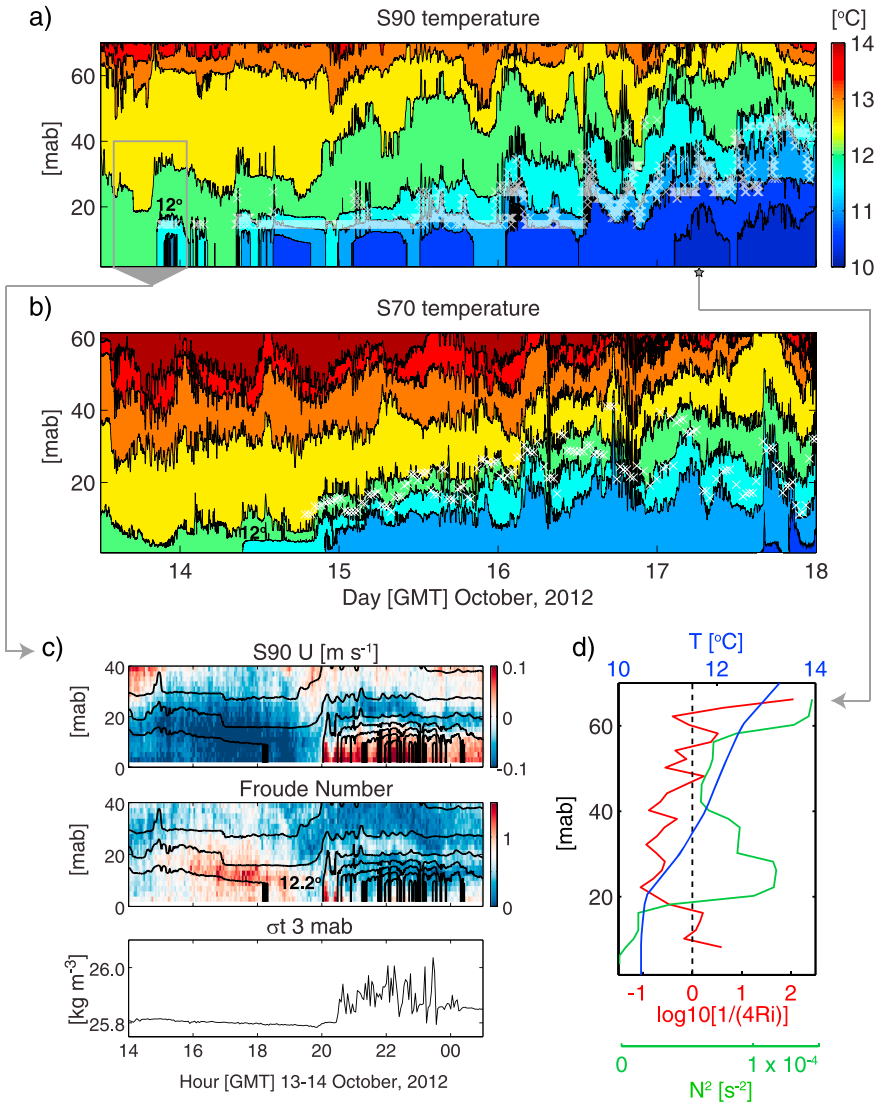

Figure 4. Temperature contours in 0.5°C steps for (a) S90 and (b) S70 during the second upwelling period, showing the near-bottom internal wave field. The approximate depth of the near-bed pycnocline is indicated in both Figures 4a and 4b by white "cross" markers. (c) The onset of the upwelling rebound, on 13–14 October, was marked by an internal tidal bore at S90, whose characteristics are shown, where the top panel is across-isobath velocity (U), the middle panel is the Froude number, Fr, and the bottom panel is density (σ_t) from 3 mab. Both the top and middle panels of Figure 4c have isotherm contours overlaid, with 0.2°C steps. (d) A representative profile from 17 October for temperature (blue), the Richardson number (red), and the squared Brunt-Väisälä frequency, N^2 (green). The Ri profile is depicted as $\log_{10}[1/(4Ri)]$, so that $Ri < 0.25$ fall above the 0 line (black dashed).

period, these T-S fluctuations occurred at a semidiurnal period (Figure 3). These upwelling rebounds are, essentially, the onset of upwelling manifesting as a series of internal tidal bores or bolus-type features propagating near the seabed along the deep, secondary pycnocline (Figure 4a). During the second upwelling period, these steep bore- or bolus-type features appeared at S90 approximately every 12 h but were not discernable at S70 (Figures 4a and 4b). These bores were characterized by a steep upward isotherm adjustment causing decreases in temperature of more than 1°C in less than 10 min. The Froude number, a dimensionless ratio of the flow velocity to wave speed, was calculated as $Fr = |u/c|$, where u is the current speed at a given depth and c is the first-mode phase speed, which is approximated by the WKB method as $c = 1/\pi \int_{-H}^{0} N(z)\mathrm{d}z$ [*Chelton et al.*, 1998]. When Fr is supercritical ($Fr > 1$), the flow is too fast for waves to propagate upstream. When $Fr < 1$, propagation is faster than the flow and wave motions can exist [*Holloway*, 1987; *Xu et al.*, 2011]. During the downward phase of the internal tide that preceded the

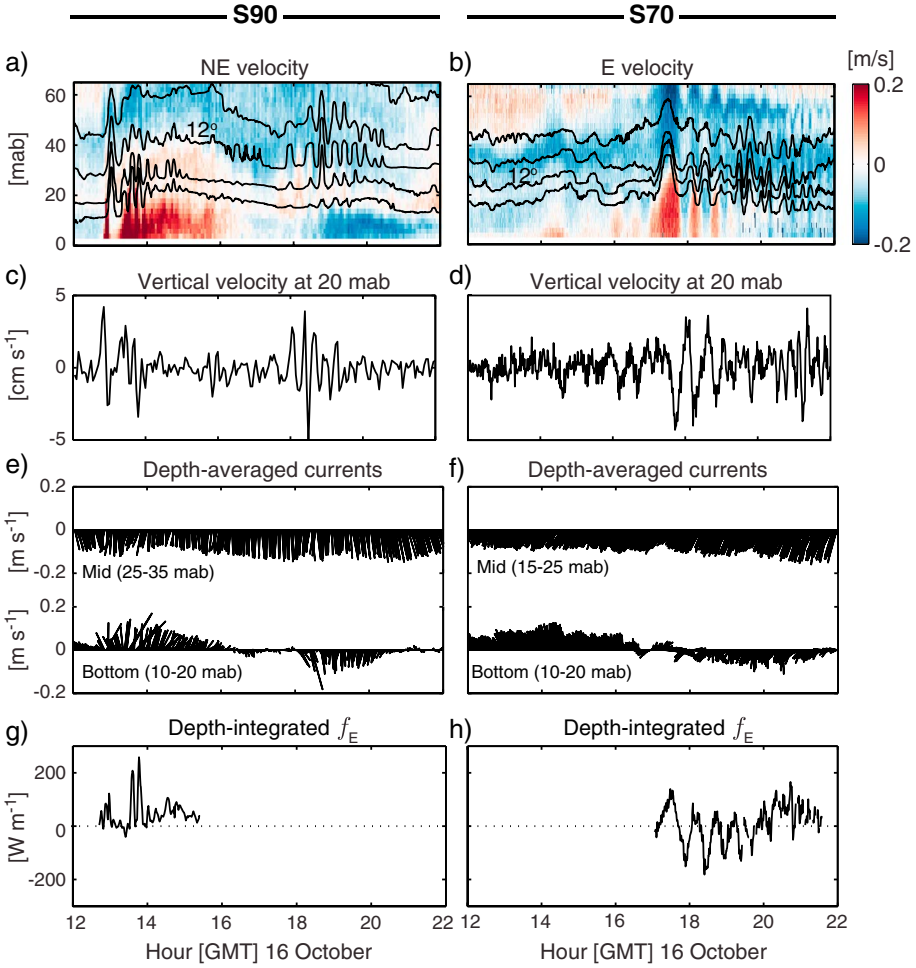

Figure 5. A 10 h time series from 16 October showing packets of high-frequency, nonlinear IWOE at (left) S90 and (right) S70. (a, b) Current velocity along the principal axis for each wave packet, with 0.5°C interval isotherms overlaid; (c, d) vertical velocity at 20 mab; (e, f) middle and near-bottom depth-averaged currents; (g, h) depth-integrated energy flux f_E associated with each wave packet.

appearance of the steep internal bores, vigorous downslope (northwestward) near-bed currents and deepening isotherms produced supercritical *Fr* conditions near the seafloor (Figure 4c). Near-bed critical Froude conditions preceding the appearance of internal tidal bores has also been reported by *Prichard and Weller* [2005] for the New England shelf, as well as by *Cheriton et al.* [2014] for this same southern Monterey Bay shelf region. The water below the near-bed pycnocline, in the "interior" of the bores, was dense, relatively homogeneous, and prone to instabilities ($Ri < 0.25$; Figure 4d).

The near-bed pycnocline also enabled the propagation of high-frequency IWOE, which, at S90, occurred at the heads of the bore-like features (Figure 4a). We developed an indicator for the presence of high-frequency IWOE close to the seabed using a wavelet analysis of near-bottom temperature and averaging the resulting variance time series corresponding to periods of 10–30 min. This wavelet indicator shows the occurrence of these near-bottom, high-frequency IWOE coinciding with the appearance of the secondary, near-bed pycnocline during upwelling periods (Figure 2g). These IWOE occurring within 20 m of the seabed had amplitudes of up to 24 m and periods between 6 and 45 min. Examples of two IWOE packets from S90 and S70 are shown in Figure 5. We note that, while these wave packets were observed only a few hours apart, it is not clear whether they are signatures of the same feature or are entirely separate. Nonetheless, the two IWOE packets exhibit similar flow structure: elevated vertical velocities and strong current shear, with the regions above and below the IWOE moving southward (southwestward) and northeastward (eastward), respectively, at S90 (S70).

In order to assess to what degree these IWOE are transporting energy across the shelf, we computed the total horizontal energy flux, $\mathcal{F}_E$, associated with these waves after *Moum et al.* [2007]: $\mathcal{F}_E = u(\mathrm{KE} + \mathrm{APE} + p')$, where u is the velocity along the direction of predominant current flow during each IWOE packet, KE is the kinetic energy, APE is the available potential energy due to the wave disturbance, and p' is the pressure disturbance due to the passage of the IWOE. Here we take p' to be the sum of internal hydrostatic pressure (due to isopycnal displacement), $p_h = g\int_z^H \rho' \mathrm{d}z'$, external hydrostatic pressure (caused by surface displacement due to the internal wave, η_H), $p_{\mathrm{surf}} = \rho_o g \eta_H$, and nonhydrostatic pressure (due to vertical accelerations), $p_{\mathrm{nh}} = \rho_o \int_z^H (Dw/Dt)\ \mathrm{d}z'$. The surface displacement, η_H, was estimated after *Moum and Smyth* [2006]. We calculated $\mathcal{F}_E$ along the principal axis of current flow, which was along-isobath (northeast to southwest) for S90 and across-isobath (east to west) for S70. At both S70 and S90, the individual IWOE on 16 October had peak instantaneous, depth-integrated $\mathcal{F}_E$ of 100–200 W m^{-1}, directed along-isobath toward the canyon rim (northeast) at S90 and, at S70, onshore (east) and offshore (west).

Our study sites were located in a relatively flat region of the shelf (slope ~0.006) that is described as a depositional regime for fine grain material [*Edwards*, 2002], and, as such, we would not expect these IWOE to be breaking in this region of the shelf. The Iribarren number, ξ, is a measure of the steepness of a wave to the shelf slope and has been applied to both surface and internal waves to classify the wave breaker type [*Boegman et al.*, 2005]. It is computed as $\xi = s/\sqrt{H/L_w}$, where s is the shelf slope, H is the wave amplitude, and L_w is a characteristic wave length scale. Here we estimated L_w as $L_w \simeq \frac{c}{H}\int_{t_o}^{t_1} \eta(t)dt$ [*Koop and Butler*, 1981; *Michallet and Ivey*, 1999], where $\eta(t)$ is the isotherm displacement, c is the wave phase speed, and t_o and t_1 are the time values before and after the wave where $\eta(t_o) \simeq \eta(t_1) \simeq 0$. The wave phase speed, c, was calculated using the baroclinic approximation $c = \sqrt{g' \frac{H_1 H_2}{H_1 + H_2}}$, with the reduced gravity, $g' = g(\Delta\rho/\rho)$, and H_1 and H_2 being the height of the water column above and below the wave, respectively. For the initial IWOE wave crests observed at S90 and S70 shown in Figure 5, this yielded $c \sim 0.3$ m s^{-1} for both wave crests, and $L_w = 165$ m for the S90 wave and $L_w = 384$ m for the S70 wave. With these parameters, both internal wave crests had $\xi < 0.03$, indicating that these were dissipative-type IWOE [*Aghsaee et al.*, 2010] and thus were likely not actively breaking in the area of our two study sites.

4. Discussion

There is increasing evidence that the cross-margin water column response to upwelling is a strong determinant in the ability of the internal tide to propagate into continental shelf regions. *Noble et al.* [2009] observed cross-shelf transport in the form of internal tidal bores and found that the ability of these bores to propagate into nearshore regions of the shelf was dependent on strong downcoast (equatorward) flow, which caused upward tilting isopycnals. *Washburn and McPhee-Shaw* [2013] further describe how shifts between upwelling and relaxation can directly modulate internal wave transport in the nearshore region of the California Current System, particularly in the fall season when the water column can be strongly stratified. A month-long time series from our same study site from the previous year (fall 2011) concluded that the ability of energetic internal tides to propagate over the Monterey Bay shelf is set, in part, by wind-driven shifts in stratification over the shelf [*Cheriton et al.*, 2014]. The correlation between low-frequency wind forcing and internal wave propagation also holds for the nearshore region of Monterey Bay, in that the structure and the strength of the outer shelf to midshelf stratification modulates the structure and strength of internal bores propagating in the nearshore region [*Walters et al.*, 2014]. In addition, observations from within the Monterey Submarine Canyon also indicate that different stratification regimes can result in different manifestations of the internal tide (e.g., standing or progressive wave) [*Petruncio et al.*, 1998; *Zhao et al.*, 2012; *Hall et al.*, 2014]. Our observations of the IWOE field associated with a near-bottom pycnocline also illustrate the connection between internal wave propagation and upwelling-driven stratification. During our study period, energetic, high-frequency IWOE were present near the seabed during upwelling periods, when the near-bottom pycnocline was present over the shelf (Figure 2).

In addition to the correspondence between the presence of this secondary, near-bottom pycnocline and high-frequency IWOE, we also explored the relationship between the occurrence of this near-bottom wave guide and M_2 internal tidal energy. The low-frequency variability of the internal tide in Monterey Bay appears

to be decoupled from the surface barotropic tide and is likely governed by a multitude of mesoscale and submesoscale processes [*Nash et al.,* 2012], making a prediction of the internal tide strength in the bay extremely difficult. Consequently, the presence of a wave guide alone does not guarantee energetic internal motions. Nevertheless, during our study period, the M_2 internal tidal energy in the deeper water column was depth colocated with the near-bed pycnocline; as the near-bed pycnocline shoaled, so too did the M_2 tidal energy (figure not shown). The deepest M_2 internal tidal energy peak occurred at S90 from 13–16 October, the same time period when the semidiurnal internal tidal bore/bolus-type features were observed at that site and also during the strongest and most prolonged upwelling interval during our study period.

Nonlinear internal waves are capable of efficiently transporting energy across substantial distances and thus are likely important drivers for the transport and distribution of nutrients, contaminants, sediment, planktonic organisms, and other suspended matter in the shelf and nearshore regions. The presence of a near-bed pycnocline likely enables a considerable energy transport across the shelf when strong baroclinic internal tides are incident along the Monterey Bay margin. *Carter et al.* [2005] observed downslope propagating IWOE over the southern Monterey Bay shelf and report that these IWOE accounted for 20% of the observed turbulent kinetic energy dissipation. The net (depth-integrated) energy fluxes computed for the IWOE packets on 16 October (Figure 5) were $O(1 - 10)$ kW m^{-1}. Taking this as a representative energy flux for IWOE packets that estimated to occur every 12 h, within a 3 day upwelling period $O(100)$ MJ m^{-1} of energy transport may occur over the southern continental shelf of Monterey Bay. For comparison, *Moum et al.* [2007] estimated a cumulative energy transport for the IWOE observed over the Oregon shelf of 20 MJ m^{-1} over a 48 h period. The substantial energy flux we observed occurring in the deep shelf waters of Monterey Bay would be dependent not only upon the presence of a near-bottom wave guide but also upon the availability of M_2 internal tidal energy.

The energy fluxes associated with our observed IWOE are comparable to previous observations in other shelf regions. At both of our study sites, the individual IWOE on 16 October had peak instantaneous, depth-integrated f_E of 100–200 W m^{-1}. Using observations from the Oregon shelf, *Moum et al.* [2007] report energy fluxes for IWOE that are approximately an order of magnitude greater; however, these IWOE had amplitudes nearly twice that of those we observed. Putting the energy transport of the leading solitary-type waves in units per crest length gives $O(100)$ kJ m^{-1}, which is comparable to the value reported by *Bourgault et al.* [2007] for IWOE in the St. Lawrence Estuary, Quebec.

Our observations raise several questions regarding the potential environmental impacts of a near-bottom wave guide and subsequent passage of energetic internal tides and higher-frequency IWOE. How prevalent are IWOE over the shelf? How far do these waves propagate and where do they ultimately terminate? To what degree do these internal waves affect benthic exchange processes between the seabed, BBL, and the upper water column? Further investigations into these questions will require high temporal resolution water column measurements collected over periods greater than a month at multiple sites over the middle to deep shelf.

Acknowledgments

This project was funded by the National Science Foundation (grant OCE0961810 to McPhee-Shaw, Bellingham, Shaw, and Stanton) and by the U.S. Geological Survey's Coastal and Marine Geology Program. We thank C. Hunter, T. Elfers, P. Dal Ferro, J. White, and J. Ferreira for deployment support. We are grateful to M. McManus at the University of Hawaii at Manoa for loaning us the autonomous profiler. J. Sevadjian (MLML) provided helpful discussions. B. Edwards and J. Reid supplied the mud belt sediment distribution data shown in Figure 1, and N. Golden assisted with the mapping of these data. We thank the captain and crews of the R/V *Pt Sur*. We are grateful to C. Sherwood for an initial review of the manuscript, and to B. Weller and an anonymous reviewer for their helpful comments. Use of trademark names does not imply U.S. government endorsement of product. The USGS data sets presented herein can be obtained by sending a written request to the corresponding author.

The Editor thanks Glen Carter and an anonymous reviewer for their assistance in evaluating this paper.

References

Aghsaee, P., L. Boegman, and K. G. Lamb (2010), Breaking of shoaling internal solitary waves, *J. Fluid Mech.*, doi:10.1017/S002211201000248X.

Boegman, L., G. N. Ivey, and J. Imberger (2005), The degeneration of internal waves in lakes with sloping topography, *Limnol. Oceanogr.*, *50*, 1620–1637.

Bogucki, D., T. Dickey, and L. G. Redekopp (1997), Sediment resuspension and mixing by resonantly generated internal solitary waves, *J. Phys. Oceanogr.*, *27*, 1181–1196.

Bourgault, D., M. D. Blokhina, R. Mirshak, and D. E. Kelley (2007), Evolution of a shoaling internal solitary wavetrain, *Geophys. Res. Lett.*, *34,* L03601, doi:10.1029/2006GL028462.

Carter, G. S., M. C. Gregg, and R.-C. Lien (2005), Internal waves, solitary-like waves, and mixing on the Monterey Bay shelf, *Cont. Shelf Res.*, *25*, 1499–1520.

Chelton, D. B., R. A. deSzoeke, and M. G. Schlax (1998), Geographical variability of the first baroclinic Rossby radius of deformation, *J. Phys. Oceanogr.*, *28*, 433–460.

Cheriton, O. M., E. E. McPhee-Shaw, W. J. Shaw, T. P. Stanton, J. B. Bellingham, and C. D. Storlazzi (2014), Suspended particulate layers and internal waves over the southern Monterey Bay continental shelf: An important control on shelf mud belts?, *J. Geophys. Res. Oceans*, *119*, 428–444, doi:10.1002/2013JC009360.

Edwards, B. D. (2002), Variations in sediment texture on the northern Monterey Bay National Marine Sanctuary continental shelf, *Mar. Geol.*, *181*, 83–100.

Fu, K.-H., Y.-H. Wang, L. St. Laurent, H. Simmons, and D.-P. Wang (2012), Shoaling of large-amplitude nonlinear internal waves at Dongsha Atoll in the northern South China Sea, *Cont. Shelf Res.*, *37*, 1–7.

Hall, R. A., M. H. Alford, G. S. Carter, M. C. Gregg, R.-C. Lien, D. J. Wain, and Z. Zhao (2014), Transition from partly standing to progressive internal tides in Monterey Submarine Canyon, *Deep Sea Res., Part II*, *104*, 164–173.

Holloway, P. E. (1987), Internal hydraulic jumps and solitons at a shelf break region on the Australian North West shelf, *J. Geophys. Res.*, *92*, 5405–5416, doi:10.1029/JC092iC05p05405.
Klymak, J. M., and J. N. Moum (2003), Internal solitary waves of elevation advancing on a shoaling shelf, *Geophys. Res. Lett.*, *30*(20), 2045, doi:10.1029/2003GL017706.
Koop, C. G., and G. Butler (1981), An investigation of internal solitary waves in a two-fluid system, *J. Fluid Mech.*, *112*, 225–251.
Lamb, K. G. (2014), Internal wave breaking and dissipation mechanisms on the continental slope/shelf, *Annu. Rev. Fluid Mech.*, doi:10.1146/annurev-fluid-011212-140701.
Mann, K. H., and J. R. N. Lazier (2006), *Dynamics of Marine Ecosystems: Biological-Physical Interactions in the Oceans*, Blackwell, Malden, Mass.
Michallet, H., and G. N. Ivey (1999), Experiments on mixing due to internal solitary waves breaking on uniform slopes, *J. Geophys. Res.*, *104*, 13,467–13,477, doi:10.1029/1999JC900037.
Moum, J. N., and W. D. Smyth (2006), The pressure disturbance of a nonlinear internal wave train, *J. Fluid Mech.*, *558*, 153–177.
Moum, J. N., J. M. Klymak, J. D. Nash, A. Perlin, and W. D. Smyth (2007), Energy transport by nonlinear internal waves, *J. Phys. Oceanogr.*, *37*, 1968–1988, doi:10.1175/JPO3094.1.
Nash, J. D., E. L. Shroyer, S. M. Kelly, M. E. Inall, T. R. Duda, M. D. Levine, N. L. Jones, and R. C. Musgrave (2012), Are any coastal internal tides predictable?, *Oceanography*, *25*, 80–95, doi:10.5670/oceanog.2012.44.
Noble, M., B. Jones, P. Hamilton, J. Xu, G. Robertson, L. Rosenfeld, and J. Largier (2009), Cross-shelf transport into nearshore waters due to shoaling internal tides in San Pedro Bay, CA, *Cont. Shelf Res.*, *29*, 1768–1785.
Orr, M. H., and P. C. Mignerey (2003), Nonlinear internal waves in the South China Sea: Observation of the conversion of depression internal waves to elevation internal waves, *J. Geophys. Res.*, *108*(C3), 3064, doi:10.1029/2001JC001163.
Petruncio, E. T., L. K. Rosenfeld, and J. D. Paduan (1998), Observations of the internal tide in Monterey Canyon, *J. Phys. Oceanogr.*, *28*, 1873–1903.
Pineda, J. (1999), Circulation and larval distribution in internal tidal bore warm fronts, *Limonol. Oceanogr.*, *44*(6), 1400–1414.
Prichard, M., and R. A. Weller (2005), Observations of internal bores and waves of elevation on the New England inner continental shelf during summer 2001, *J. Geophys. Res.*, *110,* C03020, doi:10.1029/2004JC002377.
Rosenfeld, L. K., F. B. Schwing, N. Garfield, and D. E. Tracy (1994), Bifurcated flow from an upwelling center: A cold water source for Monterey Bay, *Cont. Shelf Res.*, *14*, 931–964.
Scotti, A., and J. Pineda (2004), Observation of very large and steep internal waves of elevation near the Massachusetts coast, *Geophys. Res. Lett.*, *31*, L22307, doi:10.1029/2004GL021052.
Storlazzi, C. D., M. A. McManus, and J. D. Figurski (2003), Long-term, high-frequency current and temperature measurements along central California: Insights into upwelling/relaxation and internal waves on the inner shelf, *Cont. Shelf Res.*, *23*, 901–918.
Torrence, C., and G. P. Compo (1998), A practical guide to wavelet analysis, *Bull. Am. Meteorol. Soc.*, *79*, 61–78.
Walters, R. K., C. B. Woodson, P. R. Leary, and S. G. Monismith (2014), Connecting wind-driven upwelling and offshore stratification to nearshore internal bores and oxygen variability, *J. Geophys. Res. Oceans*, *119*, 3517–3534, doi:10.1002/2014JC009998.
Washburn, L., and E. McPhee-Shaw (2013), Coastal transport processes affecting inner-shelf ecosystems in the California Current System, *Oceanography*, *26*(3), 34–43.
Xu, J., J. Xie, and S. Cai (2011), Variation of Froude number versus depth during the passage of internal solitary waves from the in-situ observation and a numerical model, *Cont. Shelf Res.*, *3*(1), 1318–1323.
Zhao, Z., M. H. Alford, R.-C. Lien, M. C. Gregg, and G. S. Carter (2012), Internal tides and mixing in a submarine canyon with time-varying stratification, *J. Phys. Oceanogr.*, *42*, 2121–2142.